Article Title
Indirect monitoring of vortex-induced vibration of suspension bridge hangers

Authors
Daniel Cantero
Ole Øiseth
Anders Rønnquist

Manuscript version
Post-print = Final draft post-refereeing, before copy-editing by journal

DOI:
10.1177/1475921717721873

Reference:

Cantero, D., Øiseth, O., Rønnquist, A., (2017). Indirect monitoring of vortex-induced vibration of suspension bridge hangers. *Structural Health Monitoring*, 2017.

Title
Indirect monitoring of vortex-induced vibration of suspension bridge hangers

Authors
Daniel Cantero (1)
Ole Øiseth (1)
Anders Rønnquist (1)

Affiliations
(1) Department of Structural Engineering, Norwegian University of Science & Technology NTNU, Trondheim, Norway

Abstract
Wind loading of large suspension bridges produces a variety of structural responses, including the Vortex-Induced Vibrations (VIVs) of the hangers. Because it is impractical to monitor each hanger, this study explores the possibility of assessing the presence of these vibrations indirectly by analyzing the responses elsewhere on the structure. To account for the time-varying nature of the wind velocity, it is necessary to use appropriate time-frequency analysis tools. The Continuous Wavelet Transform and the Short-Term Fourier Transform are used here to obtain clear correlations between the vortex shedding frequency and the energy content of the Hardanger Bridge responses. The analysis of recorded signals from a permanent monitoring system installed on the deck and a temporary system installed on some of the hangers shows that it is possible to indirectly detect hanger-related VIVs from the deck response. Furthermore, this study elaborates on the detection of the two types of VIVs (Cross-Flow and In-Line), the spatial variability of the results, as well as a possibility to automate the detection process. The ideas reported can be implemented readily in existing SHM systems for large cable-supported structures not only to identify VIVs but also to gain a better understanding of their structural response.

Keywords
Vortex shedding, Monitoring, Cable, Hanger, Bridge, Signal processing, Time-frequency analysis

1. Introduction

Recently, every new large bridge project has also included some type of permanent monitoring system. Examples of such systems in cable-stayed bridges and suspension bridges can be found in Brownjohn et al.,[1] Andersen and Vesterinen,[2] and Li and Ou.[3] Vibration-Based Monitoring (VBM) consists of the recording, storage and analysis of the dynamic behavior of these large structures. VBM has been shown to be a valuable source of information for many practical uses, including the characterization of the bridge response under different loading conditions, structural performance evaluation, validation and correction of design models and source of structural updating information.[1] To facilitate the analysis, it is necessary to obtain a proper understanding of all the underlying dynamic phenomena present in the recorded signals.

Wind loading is one of the major concerns in the design of long-span bridges.[4] Among the many possible wind phenomena that need to be considered, Vortex-Induced Vibrations (VIVs) excite the structure subject to low to moderate wind velocities. When the wind flow encounters a bluff body (here, a cable), the stream is separated in the wake of the structural member, creating a Von Karman vortex trail.[5] As a result, this phenomenon produces a periodic oscillation that can be characterized by the vortex shedding frequency f_{vs} (Eq. (1)), where *U* is the wind velocity, *St* the Strouhal number, and *D* the diameter of the cylinder. When this excitation frequency is close to one of the structure's frequencies, a synchronization appears between the loading and the response, which is generally called the lock-in phenomenon. This has been reported in several cable-supported bridges (either cable-stayed or suspension bridges) producing vibrations on the cables that required the installation of mitigation measures.[5,6]

$$f_{vs} = \frac{U\,St}{D} \qquad \text{Eq. (1)}$$

Since the seminal work by Vickery and Basu,[7,8] the VIVs of bluff bodies have been studied extensively, Wu and Kareem[9] and Williamson and Govardhan[10] being two good review works on the topic. However, there is still no full analytical description available even for the simplest cylindrical shape,[11] and large discrepancies are reported between empirical tests and predictions from different computational codes.[12] Nevertheless, knowledge about this phenomenon has been gained over the years. In particular, it has been found that VIVs can be divided into two distinct motions. The first type is Cross-Flow (CF) vibrations that correspond to movements of the member perpendicular to the wind direction. In-Line (IL) vibrations are the second type of VIV motions and are produced along the direction of the wind stream. IL motions are strongly coupled to CF motions[12] and have a frequency ratio of approximately two[9,13] for cylindrical bodies. In other words, if the CF vibration of a cable is f_{vs}, then the IL motions vibrate at a frequency of $2f_{vs}$ but in general with a lower intensity.[9]

Due to the fluctuating nature of wind velocity, the vortex shedding frequency f_{vs} (Eq. (1)) also varies continuously, thereby producing a non-stationary excitation on the cable. Therefore, it is advantageous to study this phenomenon using Time-Frequency (TF) analysis tools. However, only a few studies have embraced this fact when investigating VIVs. For instance, some early work by Matsumoto et al.[14] studied the non-stationary characteristics of the cable response in a wind tunnel using wavelet analysis. More recently, some additional wavelet analysis has been performed on signals from an experimental setup in Chen et al.[15] or based on results generated in numerical simulations.[13] Other TF techniques, such as the S-

Transform in Li et al.,[16] which can be related to the wavelet transform,[17] have also been used in the field.

VIVs are self-exciting but also self-limiting phenomena[11] and exhibit limit cycle oscillations[9] due to nonlinear fluid-structure interactions. These vibrations generally excite higher modes of the cable with relatively low displacement amplitudes,[18] rarely attaining vibration magnitudes greater than half the cable diameter.[5] On the other hand, the acceleration amplitudes may be significant because of the high oscillation frequencies.[18] Although these vibrations might not produce devastating damage to the cables,[15] it can induce additional stresses and seriously alter the fatigue life of cables and connections.[9]

In a long-span cable-supported bridge, the overall structural dynamic response cannot be uncoupled from the dynamics of its cable system.[4] Consequently, the effects of wind on the cables influence the dynamic behavior of the remainder of the structure. This paper confirms this statement using measurements from the Hardanger suspension bridge (Norway) and shows that it is possible to indirectly study VIVs on hangers when inspecting the response elsewhere on the structure. Figure 1 schematically presents the effect of wind (in blue) when it encounters a bluff body (the hanger), therein producing a vortex trail in the wake of the cable. Note that, for clarity, only the wind and vortex shedding trail for one hanger are shown in Figure 1, but similar effects are expected in the remainder of the hangers. These alternating wind forces lead not only to the VIV of the hanger itself but also to detectable vibrations on the bridge's deck. To identify the wind-induced vibrations, the recorded signals are analyzed using appropriate TF techniques to precisely account for the non-stationary nature of the response. In particular, two TF techniques are employed: the Continuous Wavelet Transform (CWT) and the Short-Term Fourier Transform (STFT). The results presented here show that it is possible to obtain additional and valuable information from existing monitoring systems on large bridge structures. Furthermore, a careful analysis in the TF domain highlights relevant features in the signals that enable a better understanding of the signal's content and thus facilitates the proper monitoring of the structure.

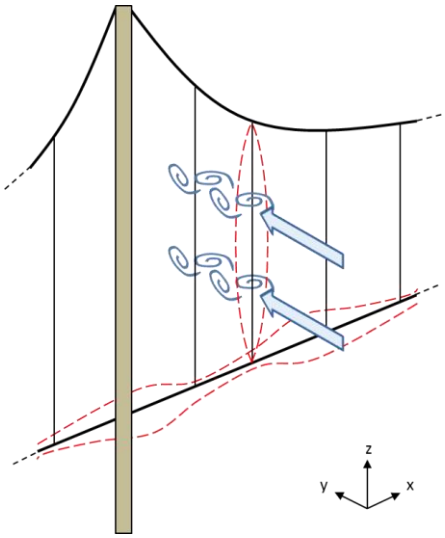

Figure 1: Schematic representation of Vortex Shedding at the hanger (Blue) and Vortex-Induced Vibrations at the hanger and deck (Red).

This document starts with the description of the studied bridge and the two types of installed instrumentations, namely, permanent and temporary. The first type is the original monitoring system of the bridge, and the second type corresponds to an additional system

installed on some hangers only temporarily for this study. The following section directly investigates the VIVs of the hangers based on TF analysis. Then, Section 4 studies the signals from the permanent system to indirectly detect hanger-induced vibrations. This is supported with some additional results regarding the two types of VIVs, the spatial variability of the results and the possible automation of the analysis. Finally, the last section is a discussion where the authors elaborate on the strengths, difficulties and further possibilities of the proposed methodology.

2. Hardanger Bridge

The suspension bridge under investigation in this study is the Hardanger Bridge (Figure 2a), which has a central span of 1310 m. This is the longest suspension bridge in Norway and was among the top-10 longest suspension bridges in the world when completed in 2013. The bridge only has two traffic lanes and one lane for bicycles and pedestrians, which is unusually narrow, making it one of the slenderest long-span suspension bridges worldwide. The width of the girder is 18.3 m, and the distance between the two main cables is only 14.5 m. Wind tunnel testing of scale models of the bridge were performed during its design and highlighted the need for remedies to avoid VIVs of the deck. This was achieved by introducing guide vanes as an integrated aspect of the bridge's cross-section.[11] The final design accounted for a 10-min mean wind velocity of up to 38 m/s, corresponding to a return period of 50 years. The cable system is composed of two main cables with a diameter of 600 mm, each anchored to the abutments, as well as vertical hangers that connect the deck to the main cables. There are 65 hangers on each side, with lengths of up to 127 m and consisting of locked coil strands of galvanized steel wires (Figure 2b) covered by a protective paint with a diameter of 68 mm. Thus, each hanger is a bluff body exposed to wind currents, shaped as a cylinder.

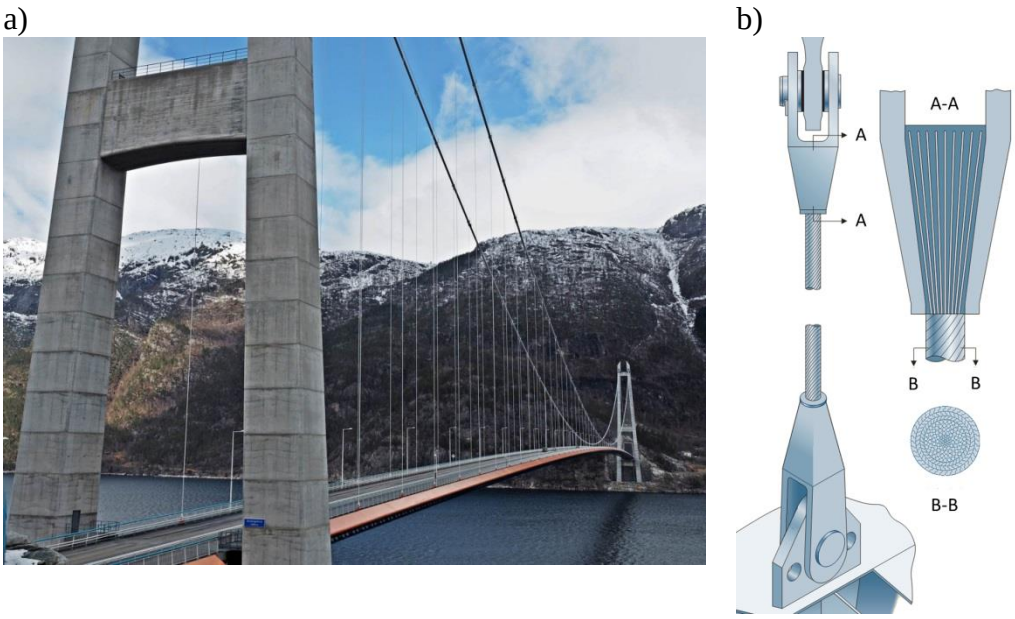

Figure 2: a) Hardanger Bridge; b) Detailed view of hanger

2.1 Permanent monitoring system

The Hardanger Bridge is equipped with a permanent monitoring system with the main goal of surveying the wind loading and observing the structural dynamic behavior. The system consists of 20 triaxial accelerometers and 9 ultrasonic anemometers distributed along the

deck and pylons, as shown in Figure 3. The signals are stored locally but are also sent wirelessly to a server on-line, where they can be downloaded and processed from any computer. For a more detailed description of the permanent monitoring system, the reader is referred to Fenerci et al.[19] Additionally, this study performs the modal analysis of the bridge and investigates the long-term buffeting response. The results show that the relevant bridge modes and its response due to buffeting are limited to the low frequency (0-1 Hz) range.

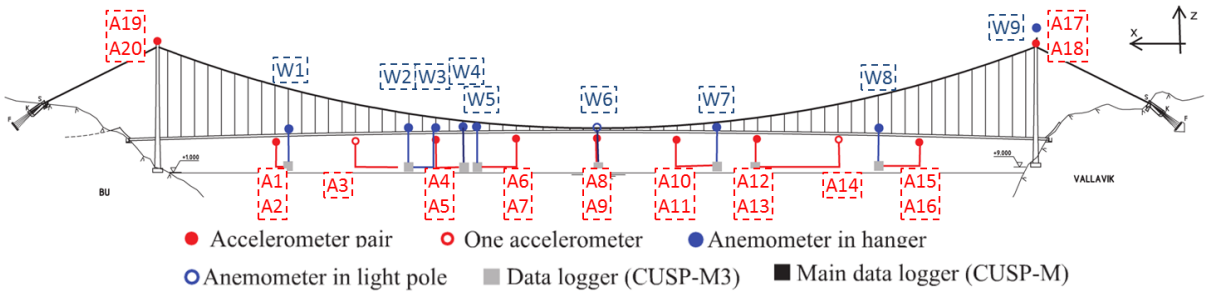

Figure 3: Layout of permanent monitoring system

2.2 Temporary measurement

In addition to the permanent monitoring system, a complementary temporary measurement campaign was performed, which consisted of the direct measurement of accelerations on the hangers. The two longest hangers (127 m and 119 m) near the north pylon and on the sidewalk side were carefully investigated. Measurements were performed during two days with different weather conditions; while Day 1 was sunny and almost without any wind gusts, Day 2 was colder, with wind velocities reaching 15 m/s. Two types of experiments were performed: impact hammer testing and 1-hour ambient vibration measurements. The experiments with the hammer were performed on both hangers only during Day 1, with the idea of extracting precise information about the hangers' dynamic properties. The ambient vibration measurements were performed on both hangers and repeated both days, thereby providing supporting data for structural identification for different weather conditions. The instrumentation used consisted of a 5.5 kg ICP impact hammer and 3 ICP triaxial accelerometers connected to a National Instruments CompactDAQ module, which logged the signals directly to a laptop. The accelerometers were installed at various locations; one was fasten to the hanger, a second sensor was attached to the deck below the hanger, and the third sensor was installed at the connection between the hanger and deck (see Figure 4). During the impact hammer testing, the location of the accelerometer on the hanger was raised to 12 m, and several hit locations were recorded along the hangers in 2 m intervals.

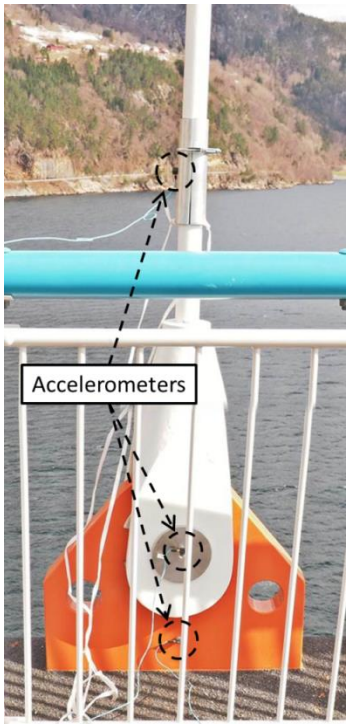

Figure 4: Accelerometers on hanger

The analysis of the impact hammer measurements provides robust and consistent values of the hanger frequencies. However, when the results are compared to the values obtained during ambient vibration, there is a clear discrepancy. Figure 5 compares some frequencies extracted from the hammer test procedure and the Power Spectral Densities (PSD) of the ambient vibration signals for different days. After verifying the measurements and calculations, it was concluded that the variations in the frequencies result from changes in temperature. For a restrained tensioned cable, such as the hanger, the thermal loading due to changes in ambient temperature produce variations in cable tension that are reflected in significant changes in frequencies.[20] The magnitude of the frequency variation depends on the geometric, thermal and mechanical properties of the member. For illustrative purposes, Table 1 shows the theoretical variations in some of the hanger's natural frequencies, modelled as an independent simply supported beam (for a 127 m long cable with Young's modulus = 290 MPa and coefficient of thermal expansion = $13 \cdot 10^{-6}$ $°C^{-1}$). This model is only a rough approximation of the real behavior of the hanger and bridge system under temperature effects, but provides a good indication of the amount of frequency variations to expect.

Although the hammer test and one of the ambient vibration tests were performed on the same day (Day 1), they were not performed simultaneously. This meant that, between the few hours difference between readings, there was a slight increase in ambient temperature, which lead to a small shift in the frequencies (compare the dashed line results to the blue line peaks in Figure 5). Even larger frequency shifts were obtained from the ambient vibration results on Day 2 (red line in Figure 5). The variations observed in Figure 5 agree well with the theoretical expected frequency variations due to two small temperature increments (one positive and one negative) listed in Table 1 agree.

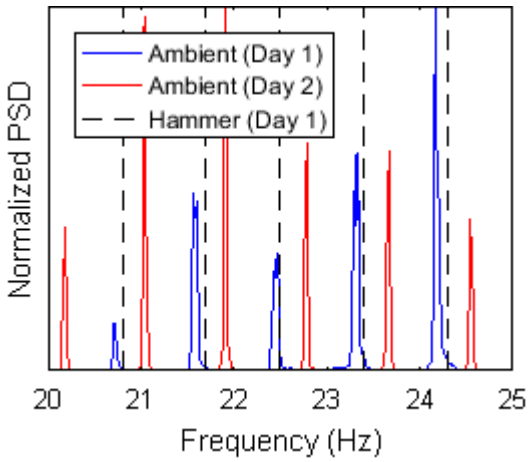

Figure 5: Influence of temperature on hanger frequencies. PSD of two different days

Table 1: Theoretical frequency changes due to small temperature variations

Measured frequency (Hz)	20.80	21.70	22.50	23.40	24.30
Expected frequency (Hz) for $\Delta T = +1$ °C	20.67	21.57	22.36	23.26	24.15
Expected frequency (Hz) for $\Delta T = -2$ °C	21.05	21.96	22.77	23.68	24.59

Several interesting results and conclusions can be drawn already from this detailed inspection of the hanger frequencies. As expected, the cable has a large number of closely spaced frequencies separated by less than 1 Hz. But more importantly, the analysis shows that these frequencies are not fixed and do vary with the ambient temperature, even over the course of a day. It is common practice to study VIVs in terms of the so-called reduced (wind) velocity, which is equivalent to the reciprocal of the Strouhal number (*St*) and thus depends on the frequency (see Eq. (1)). However, as noted in Matsumoto et al.,[14] the existence of multiple frequencies requires the definition of multiple reduced velocities, one for each mode of vibration. This fact, together with the changing nature of the frequencies with temperature, makes the definition of the reduced velocity impractical in this case and is not further used in this study.

An important parameter that determines the magnitude of the VIVs is the intrinsic structural damping of the excited member. The oscillatory loading generated by the vortex shedding phenomenon at the wake of the hanger does not induce significant vibrations if the excited mode is sufficiently damped. The Scruton number (*Sc*) is generally used to assess the risk of violent VIVs,[5] where smaller values indicate higher risk. The Scruton number for mode-i is defined in Eq. (2), where δ_i is the logarithmic decrement of the same mode, m is the mass per unit length, ρ is the air density, and D is the diameter of the cylinder.

$$Sc_i = \frac{2\delta_i m}{\rho D^2} \qquad \text{Eq. (2)}$$

With the hammer test measurements, damping estimates are obtained with the line-fit method.[21] Figure 6 shows the extracted damping values for Hanger 2 (119 m). Because the hammer measurements were repeated several times, Figure 6 shows multiple damping estimates and identifies the value that corresponds to the result that provides the best fit. Extracting accurate damping values from experimental measurements is in general not straightforward and prone to large deviations. This is even more problematic for systems with closely spaced modes. Thus, the damping values presented here should only be taken as

indicative; however, similar results have been reported previously.[18] The results show a clear trend indicating that hanger damping is in general very low and that it tends to decrease for higher modes, which can be regarded as mass-proportional damping. Although not shown here, Hanger 1 (127 m) features similar damping estimates. Therefore, because of the low damping values, significant VIVs and the appearance of lock-in phenomena can be expected on the studied hangers. Lower modes of vibration have sufficient internal damping to dissipate the wind energy input, avoiding the appearance of VIVs.

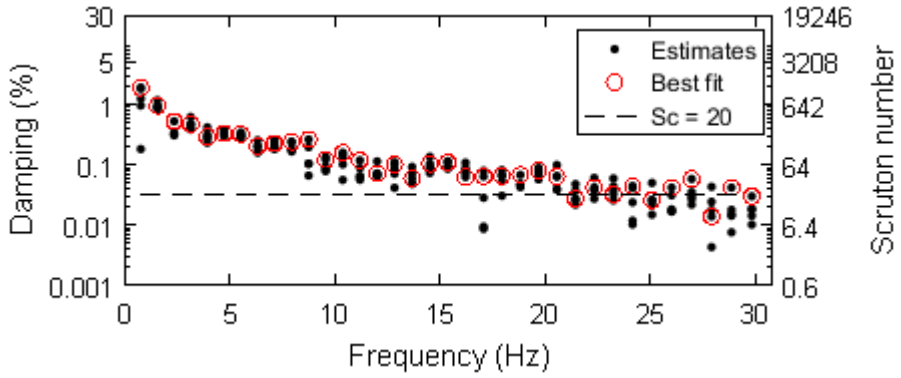

Figure 6: Hanger 2 (119 m) damping estimates

Figure 6 also shows the equivalent Scruton numbers for the displayed damping values, assuming material densities of 7800 kg/m^3 for steel and 1.2 kg/m^3 for air. It is generally acknowledged that there is no risk of VIVs when $S_c > 20$.[5] According to Figure 6, this would suggest that only the frequencies above 20 Hz are capable developing large VIVs. However, this document reports (in following sections) instances of VIVs for frequencies as low as 6 Hz. This discrepancy might be explained because in the literature the definitions of the Scruton number and the mentioned limit have been determined considering the first mode of a system. Alternative definitions might be necessary to study VIVs related to higher modes of vibration, but are out of the scope of this study.

3. VIV on hanger

This section investigates VIVs of the hanger by directly analyzing the recorded acceleration signals on the cable during the ambient vibration measurements (1 h) on Hanger 2 (119 m) during Day 2. During that period, strong and variable winds were measured at the closest anemometer to the hanger (Figure 7). The anemometers are located 8 m above the bridge deck, which is on average 50 m above the water. Therefore, an approximately constant magnitude free field wind can be expected along the vertical dimension, only disturbed by the turbulences produced by the hangers. To remove the large variability due to wind gusts, a 60 s average value is taken as representative of the instantaneous wind velocity (Figure 7a), observing velocities between 5 m/s and 11 m/s The horizontal wind direction, presented in Figure 7b, is not perpendicular to the main bridge axis but remains approximately constant during the duration of the measurements. As for the turbulence intensity (Figure 7c) larger variations have been recorded, obtaining values between 7 % and 20 %.

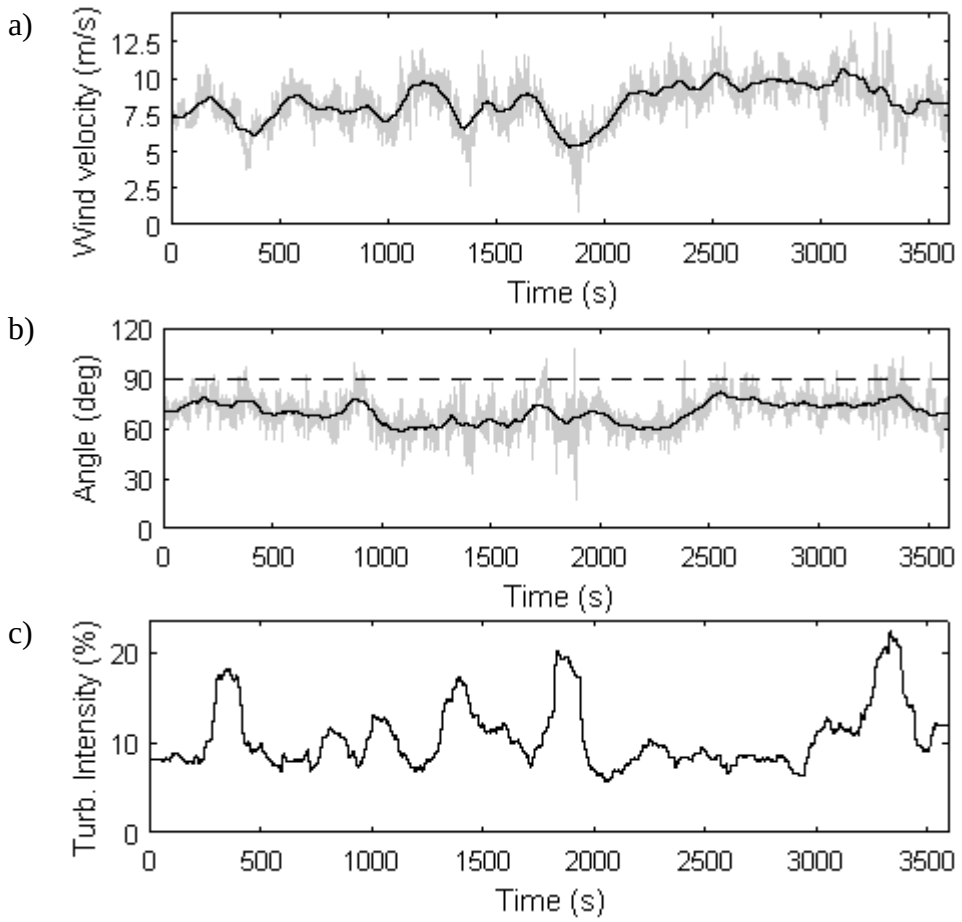

Figure 7: Time histories of wind properties; a) Wind velocity (gray = raw data, black = 60 s average); b) Horizontal angle with respect to main bridge axis (gray = raw data, black = 60 s average, dashed = perpendicular to bridge); c) Turbulence intensity

Due to the time-varying nature of the excitation, the response of the hanger is non-stationary. Thus, it is convenient to analyze such signals with Time-Frequency (TF) tools. Perhaps one of the most common TF tools is the Continuous Wavelet Transform (CWT), which essentially compares scaled versions of a waveform (basis) at different time instances of the signal. As a result, the CWT offers a map of coefficients in the time and frequency domain that are proportional to the energy content of the signal. Selecting the appropriate basis for the CWT analysis is not trivial and depends on the problem at hand and the final purpose of the analysis. For this study, it is found that the Modified Littlewood-Paley basis (MLP) provides good results for visualization purposes. The reader is referred to Nagarajaiah and Basu[22] for additional explanations on the theory and characteristics of CWT analysis as well as on the definition of the MLP basis.

The acceleration signal of Hanger 2 (Figure 8a) is analyzed with the CWT and the MLP basis. The result is the time-frequency energy map shown in Figure 8b, where high energy levels are shown as dark red, gradually changing to orange and yellow for lower levels and low or no energy represented in white. For a cylinder 68 mm in diameter and a Strouhal number equal to 0.18 (see Section 3.2 for additional discussion on this particular value), the wind velocity can be transformed into the expected vortex shedding frequency using Eq. (1). Figure 8b shows the time-varying vortex shedding frequency with a dashed black line that features some abrupt changes and varies between 14 and 28 Hz. There is a clear correlation between the vortex shedding frequency produced by the wind and the energy

content of the acceleration signal. During the first 1000 s, the energy seems to be concentrated near the 20 Hz frequency band even though the vortex shedding frequency is not constant. This can be attributed to the lock-in phenomena, where small changes in excitation frequency do not translate into changes in response frequency. However, after the initial period (>1000 s), the variability of the vortex shedding frequency is sufficiently large, and there is a very good correlation between excitation and response frequencies. Note that the recorded wind velocities are obtained from an anemometer located 200 m away from the studied hanger. Thus, the actual wind velocities at the hanger might be slightly different, which would explain the small discrepancies observed between the vortex shedding frequency and energy map in Figure 8b.

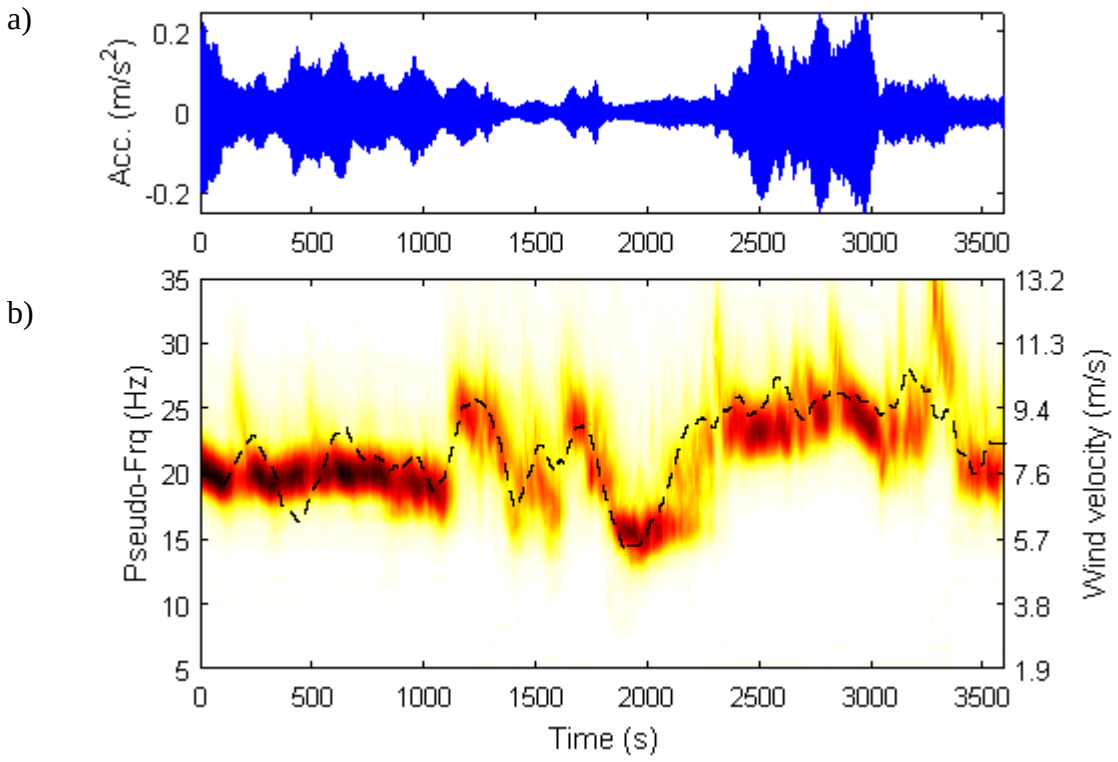

Figure 8: a) Hanger acceleration during ambient test; b) Continuous wavelet transform, dashed lines = 60 s mean wind velocity

It is important to note that the wavelet coefficients (shown in Figure 8b and in the remainder of this document) have been normalized by the instantaneous energy (obtained as the sum of all squared wavelet coefficients at a given instant). This normalization enables the direct comparison of the wavelet coefficients along the whole time series. For instance, this means that the results at 2000 s and 2500 s in Figure 8b have similar normalized wavelet coefficients even though the actual acceleration magnitude (energy) is much larger for the latter. Additionally, this normalization will prove to be useful in Section 4 when studying the acceleration signals from the deck for removing the momentarily high energy values due to passing vehicles.

3.1 Short-Term Fourier Transform

Alternatively, the TF analysis can be performed with the so-called Short-Term Fourier Transform (STFT), which essentially consists of successive Fourier transforms of overlapping portions of the signal. Each portion is obtained by windowing the original signal.

Hence, key parameters in a STFT analysis are the type of window, its length (duration) and the amount of overlap. In this study, a 10 s Hamming window was used, with a 50% signal overlap. Figure 9 shows the STFT of the same hanger ambient vibration signal analyzed in Figure 8. Compared to the CWT (Figure 8b), the STFT (Figure 9) offers a much clearer concentration of the energy near the hanger frequencies. This is particularly obvious during the lock-in part of the signal (<1000 s), where most of the energy is concentrated in a narrow band near 20 Hz. In addition, it is possible to appreciate temporary energy concentrations near 19 Hz or 21 Hz following the vortex shedding frequency produced by the wind. Thus, Figure 9 shows that the vibrations of the hanger are not concentrated only around a single mode; multiple modes are excited simultaneously at any given time. These closely spaced vibration frequencies produce typical beat-like oscillations, which can be clearly appreciated when holding the hanger directly with the hand. Note again that, in Figure 9, the small discrepancies between the vortex shedding frequency and the STFT results might be because the measured wind is 200 m away. The actual wind exciting that hanger is most likely slightly different but strongly correlated.

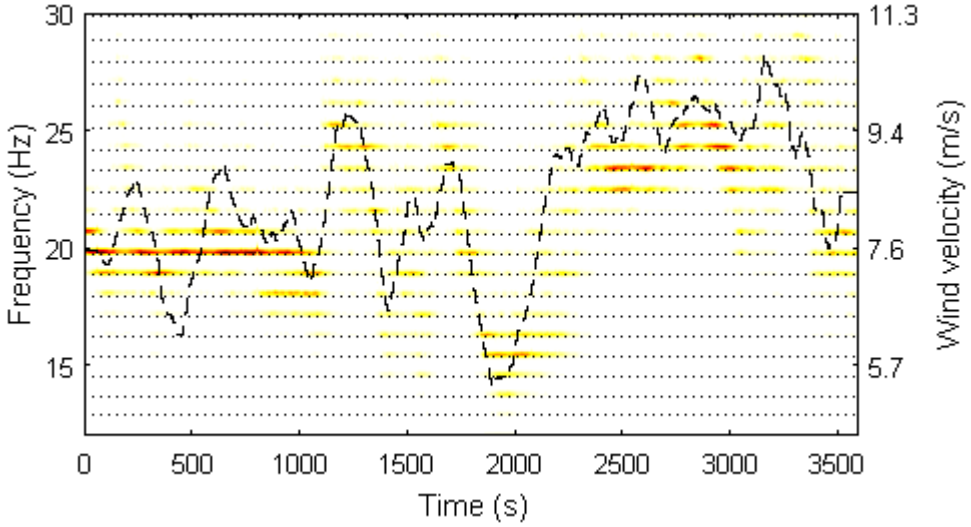

Figure 9: STFT of hanger acceleration during ambient test; dashed lines = 60 s mean wind velocity; dotted lines = extracted hanger frequencies

The differences between the time-frequency energy maps obtained with different tools are evident. For the case of the STFT (Figure 9), a better frequency resolution is obtained. The use of a sufficiently long window allows energy concentrations near individual hanger frequencies to be presented clearly. However, this reduces the time localization properties of the results. There is a greater uncertainty about when a particular frequency is excited, making it more difficult to trace rapid changes in the vortex shedding frequency. On the other hand, the CWT (Figure 8) offers a broader energy band. This is because of the particular basis used (MLP), which was originally developed to maximize, simultaneously, time and frequency localization properties.[22] It is not possible to identify individual hanger frequencies with the CWT results, but it is easier to trace the evolution of the energy content in time. Thus, both analysis methods have their strengths and drawbacks and should be used as complementary tools. Therefore, in this study, both tools have been used when deemed appropriate to maximize the usefulness of the recorded signals. In particular, the CWT is used to explore visually different phenomena in the time-frequency domain, because of its enhanced graphical representation. On the other hand, the STFT has been used in Section 4.4 when attempting to automate the VIVs identification because of the computational efficiency of the Fast Fourier Transform algorithm.

3.2 Strouhal number

At this point, it is valuable to elaborate on the actual value of the Strouhal number (*St*). It can often be seen in the relevant literature that, for practical applications, *St* for cylinders is 0.2.[5] However, over the course of this investigation, it was found that this value is only approximate, and when using it, there was a consistent offset between the vortex shedding frequency and the energy map results. Supported by multiple experimental results, Norberg[23] shows that *St* depends on the Reynolds number (*Re*). The relation for a smooth cylinder is given as a numerical expression, which for convenience is reproduced graphically in Figure 10. The Reynolds numbers for winds in the range of 1 to 30 m/s (assuming a 1.2 kg/m^3 air density and a $1.81 \cdot 10^5$ kg/m s air viscosity) are also indicated in Figure 10. In that range, *St* is approximately constant, and the exact value is 0.185. Furthermore, the surface roughness of the cylinder also influences the actual value of the *St* number. As shown in Lienhard[24] the roughness generally reduces the Strouhal number (if only slightly) in the range of Reynolds numbers corresponding to normal wind velocities. The exact value of surface roughness of the hangers is not known. Therefore, a refined value of *St* = 0.18 is used in this study because it consistently leads to god agreement between the calculated vortex shedding frequency and the acceleration frequency extracted from the signals.

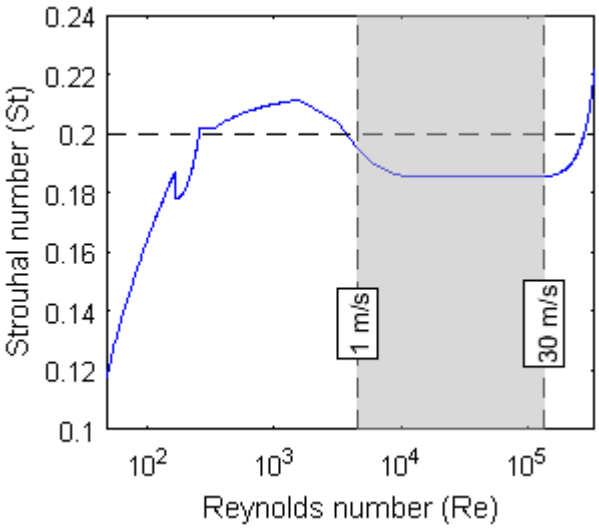

Figure 10: Strouhal number versus Reynolds number for smooth cylinder; shaded area = range of normal wind velocity

4. Effects of hanger VIVs on deck

So far this study has shown that it is possible to clearly visualize the VIV of the hanger and to correlate it with the measured wind by directly analyzing the response of the hanger. Going one step further, this section shows that it is possible to detect that very same vibration elsewhere on the bridge. As a result, it was possible to re-examine all the stored signals from the permanent monitoring system when searching for the VIVs of the hangers. The exhaustive analysis of more than 3 years of data produced some interesting results, which have been reported below.

4.1 Indirect monitoring

Figure 11a shows the longitudinal deck acceleration closest to Hanger 2 (accelerometer A16) during the same time period as for the ambient vibration test in Day 2. The analysis of this signal in the time-frequency domain produces Figure 11b. In comparison, the energy maps obtained from the direct hanger measurements (Figure 8) and deck measurements (Figure 11b) are remarkably similar. Although the direct measurements of the hanger give a much cleaner energy map, it is still possible to trace the evolution of the deck's acceleration energy and correlate it with the wind velocity. Additionally, it can be seen that the VIV of the hanger is the main source of deck vibrations in the frequency range from 5 to 30 Hz.

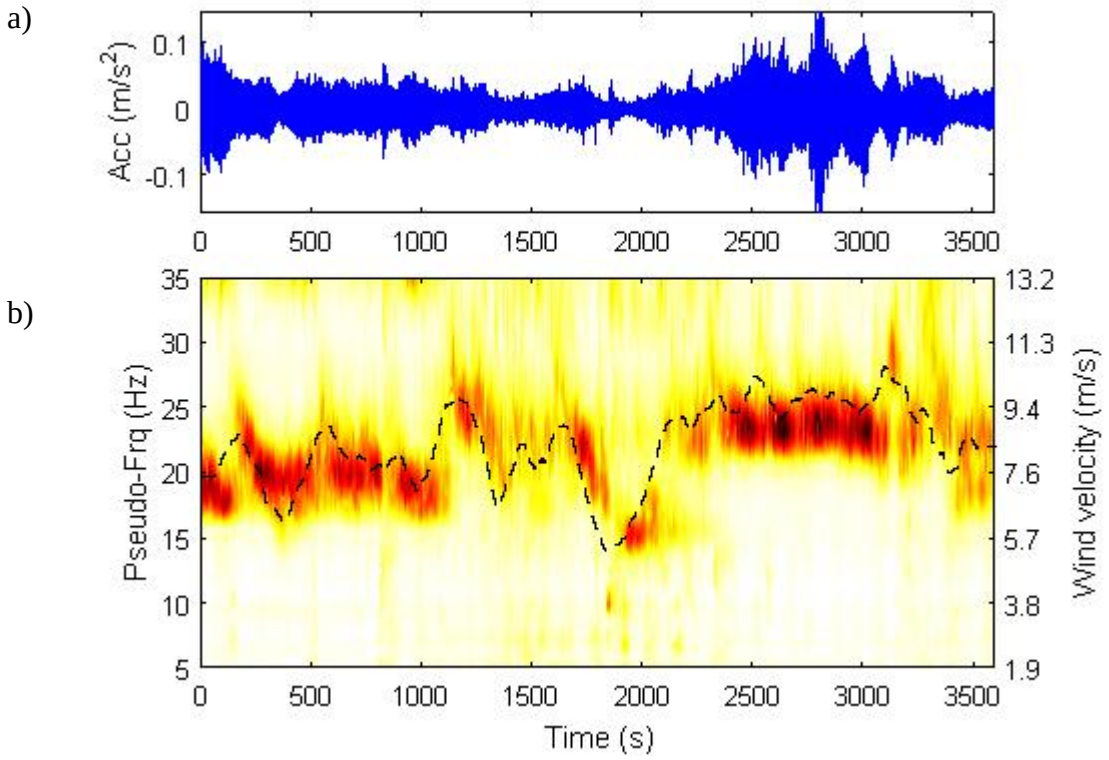

Figure 11: a) Longitudinal deck accelerations (A16) during ambient test; b) Continuous wavelet transform, (dashed lines = 60 s mean wind velocity)

It is also interesting to note that the clearest correlations between deck vibrations and hanger vortex shedding frequencies are found for the longitudinal deck accelerations. In other words, the largest vibrations on the deck due to the VIV of the hangers are in the horizontal plane along the main longitudinal axis of the bridge. This is expected because the main wind direction is generally perpendicular to the bridge, and the Cross-Flow VIV is perpendicular to that same wind stream. Thus, most of the hanger's vibrations are in the longitudinal direction and are then transmitted to the deck, as shown in Figure 11b. Nevertheless, indications of these vibrations can also be found in the other two recorded directions, namely, in the lateral (Figure 12a) and vertical (Figure 12b) deck accelerations. The lateral response of the bridge (Figure 12a) during the period 1200 s to 2300 s is dominated by a lower frequency band that cannot be attributed to VIV since no correlation with any of the recorded wind velocities could be found. Therefore, the results show that the VIV do not necessarily dominate the time-frequency maps in all directions. However, some correlation with wind velocities can often be found, to some extent, also in the lateral and vertical components.

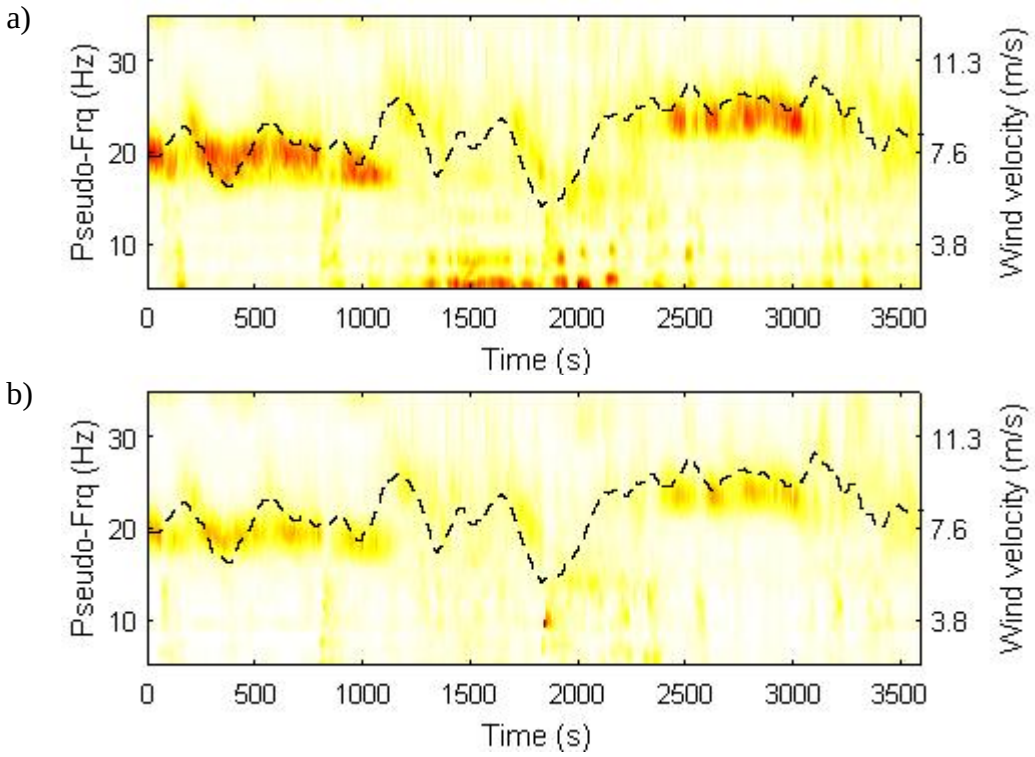

Figure 12: CWT of deck accelerations (A16) during ambient test; a) lateral component; b) vertical component (dashed lines = 60 s mean wind velocity)

4.2 Cross-Flow and In-Line VIV

As indicated in the introduction, VIVs generate motions also in the same direction as the wind, which are termed In-Line (IL). These vibrations are generally of a smaller magnitude and are characterized by a frequency that is twice the vortex shedding frequency for Cross-Flow (CF) vibrations. This subsection investigates the possibility of detecting both types of vortex-induced motions on the hanger by analyzing the signals recorded at the deck. To this end, one particularly interesting time series, characterized by calm winds interrupted by an approximately constant but higher wind velocity period, is analyzed. The CWT analysis of the two horizontal acceleration components is shown in Figure 13. As in previous sections, the CF vibrations can clearly be seen on the time-frequency energy map and are strongly correlated with wind velocity. During calm wind periods (start and end of the time series), there is no indication of vortex-related vibrations. The high Scruton numbers of the lower hanger modes (<4 Hz), as seen in Figure 6, indicate that the internal damping of the hangers hinders the development of VIVs. As soon as the wind velocity increases, clear VIV can be detected. Again, these CF vibrations are stronger for the longitudinal direction (Figure 13a) than for the lateral direction (Figure 13b). Additionally, this example shows that it is possible to identify the IL vibrations, which are expected to occur at twice the vortex shedding frequency, drawn as black dotted lines in Figure 13. In this case, the correlation between energy and (double) the excitation frequency is also evident. However, as expected, the IL vibrations are stronger in the lateral component (Figure 13b), i.e., in the direction of the wind, than in the longitudinal direction (Figure 13a).

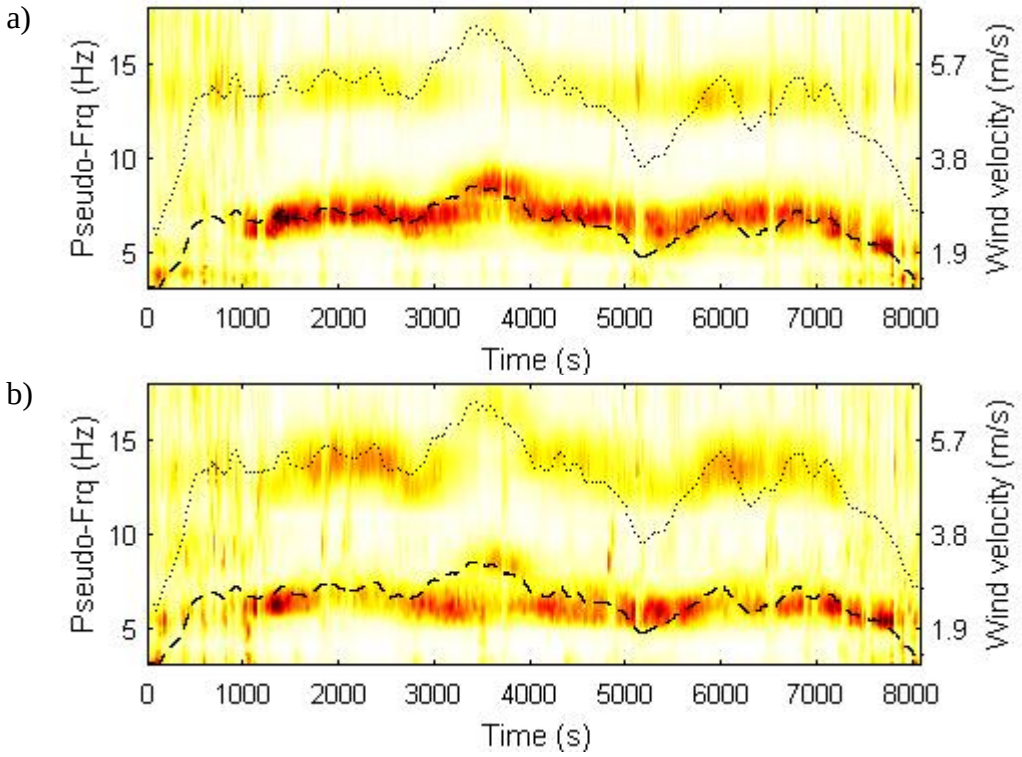

Figure 13: CWT of deck accelerations (A1) during calm-strong-calm wind period; a) longitudinal component; b) lateral component (dashed lines = 60 s mean wind velocity; dotted lines = twice the 60 s mean wind velocity)

4.3 Spatial variability

Real wind velocity fields are not uniform and are spatially dependent. Moreover, for large structures, such as the Hardanger Bridge, the air gusts can be significantly different between sections. As a result, different wind velocities can induce VIVs on different hangers along the bridge for different excitation frequencies. For instance, Figure 14a shows the CWT analysis of the deck accelerations near the south abutment for a 1-hour time series together with the vortex shedding frequency derived from the closest measured wind velocity. As reported in previous examples, there is a clear correlation between the hanger shedding frequency and deck vibrations. Similarly, Figure 14b shows wind and acceleration results near the opposite abutment. In this case, some correlation between the local wind and the acceleration is observed. However, the time-frequency map also shows a distinct energy band at approximately 22 Hz that cannot be explained by the local wind alone. In fact, to clarify the source of those unexplained vibrations, one has to consider the vibrations at the other end of the bridge. Comparing the results from the north (Figure 14b) and south (Figure 14a) abutments, the wind-induced vortex shedding frequencies are significantly different between both abutments. Furthermore, the deck vibrations recorded near the south abutment (Figure 14a) are strong enough to propagate through the whole bridge deck, thus explaining the additional band observed in Figure 14b.

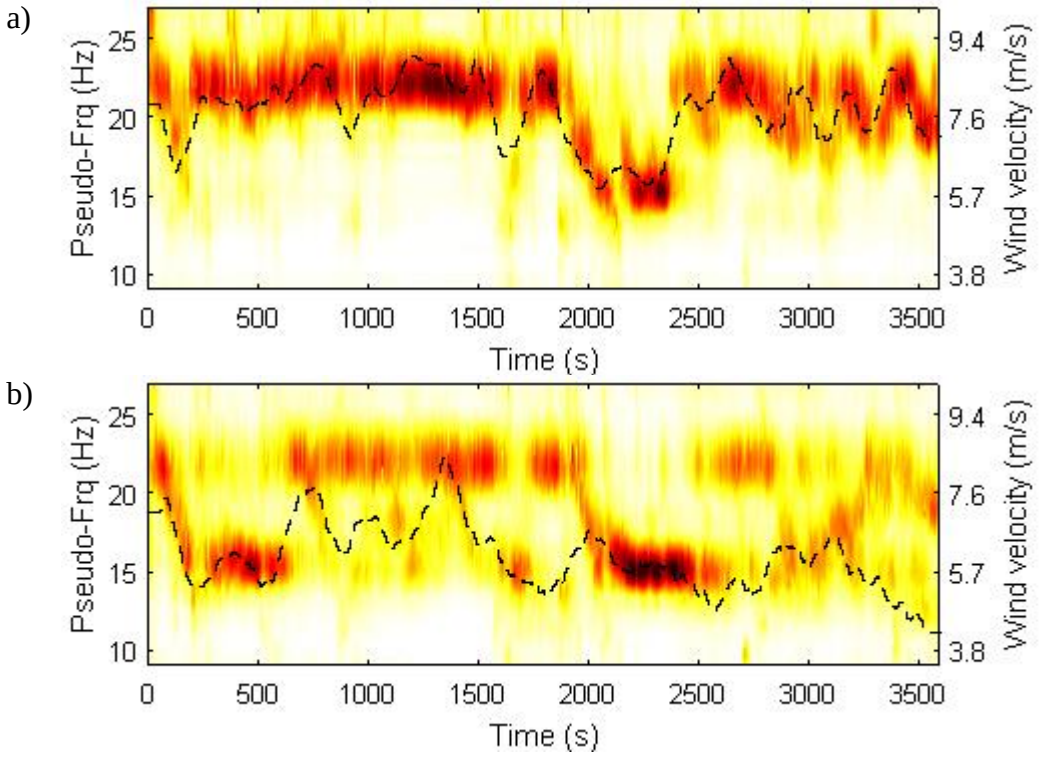

Figure 14: CWT of longitudinal deck accelerations and dashed lines = corresponding 60 s mean wind velocity; a) Accelerometer A1 and anemometer W1 near south abutment; b) Accelerometer A15 and anemometer W9 near the north abutment.

4.4 Automation

The ideas presented here have relied on visual inspection of the time-frequency energy maps. However, it would be convenient to devise some method that could be implemented programmatically to automate the process of detecting VIVs. This subsection suggests one possibility to move one step closer to that goal. The idea is to perform a STFT of the acceleration signals, which provides Power Spectral Densities (PSDs) for several time instances. Integrating these PSDs along the full frequency spectrum provides approximate values of the instantaneous energy content of a signal. Alternatively, one can integrate these PSDs only in the vicinity of the expected vortex shedding frequencies. The resulting values are estimates of the amount of energy related to VIVs.

A practical example of these ideas is shown in Figure 15 for an extended version of the calm-strong-calm time series investigated in Section 4.2 (Figure 13). The STFT is calculated without instantaneous energy normalization and for a 100 s Hamming window with a 95% overlap. Integrating it over the frequency domain yields estimates of the instantaneous total energy (Figure 15a). The results present multiple distinct spikes in energy content that correspond to vehicle passages and overall give a vague indication of higher energy levels during the stronger wind period (the range in between the dashed vertical lines). However, performing the integral only in the vicinity (a 5 Hz band) of the vortex shedding frequency leads to the results plotted in Figure 15b. The energy near the vortex shedding frequency shows a noticeable increase during the stronger wind period that has been shown to correspond to the VIVs of the hangers. Therefore, this analysis can help in highlighting situations that feature VIVs. Once these time periods have been identified, a complementary analysis in the time-frequency domain can provide additional information. In this example, to

compensate for the known spatial variation in the wind field, the following was considered: a) A sufficiently wide frequency band in the vicinity of the frequency of interest was utilized. b) The vortex shedding frequency was calculated considering the average wind velocity signals recorded along the bridge deck.

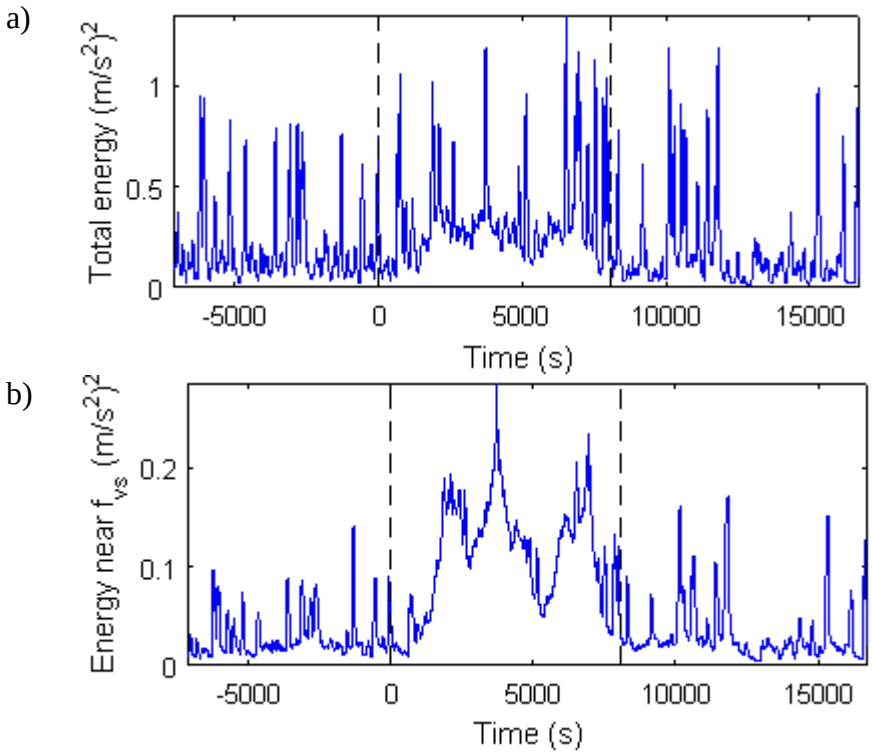

Figure 15: Deck acceleration energy content; a) Total; b) Near vortex shedding frequency (dashed lines = time range studied in Figure 13)

5. Discussion

The results in this document presented clear visualizations of the correlation between the vortex shedding frequency and the evolution of the signal's energy content, as for instance in Figure 8b. Although this might seem trivial, it already constitutes a relevant contribution of this work to the field of VIVs. Existing publications only occasionally use TF tools, which have then been used to analyze results from numerical simulation or laboratory experiments. However, to the best of the authors' knowledge, this is the first time that such clear correlations have been reported for signals recorded on a structure under normal operational conditions. The key aspect of this achievement was to identify the need for studying the problem in the time-frequency domain using appropriate tools, namely, the CWT and the STFT. Additional considerations that improved the quality of the visualizations have been the use of the normalization by the instantaneous energy as well as the choice of a coherent coloring scheme for the time-frequency energy maps.

It is acknowledged that there are other possibilities for TF analysis, such us the S-Transform and the Hilbert-Huang Transform; there might even be other wavelet bases that would yield still better results than those reported here. However, the intention of this study was not to conduct an exhaustive review of all possible TF analysis tools but rather to highlight a possible additional use of existing SHM systems. The authors explored some TF tools and reported here the methods that have worked best and fitted the purpose of the study.

In particular, the CWT is a powerful tool that has previously been successfully used in many applications and provided good time-frequency energy maps in this study. Nevertheless, this tool has shortcomings, including difficulties when analyzing low frequencies and high computational demands.[22,25] On the other hand, the STFT clearly benefits from the fast computational efficiency of the Fast Fourier Transform algorithm, which is readily available in most analysis software packages, programming languages and open-source platforms. This tool also has its own disadvantages, including the fixed frequency resolution and the need to select adequate analysis parameters (window type, duration and overlap). This is why, and as mentioned before, both tools (or any other suitable TF tool) should be used as complementary instruments rather than as exclusive and independent methods to analyze the signals.

This study has shown that it is possible to monitor the VIVs of the hangers indirectly by measuring deck accelerations and correlating them with wind velocities. Admittedly, it would certainly be very useful to be able to identify the precise hangers that feature large VIVs at any given moment. However, it can be argued that this task is extremely difficult, if not impossible, without directly monitoring each hanger. First, because of the spatial variability of the wind field, the structure is subjected to different wind speeds in different locations. This produces not only the appearance of VIVs with different frequencies for different hangers but also the possibility of multiple VIVs along individual hangers. Additional complications are not only the sheer number of hangers but also the large amount of closely spaced frequencies characterizing each hanger, together with their dependence on ambient temperature. All of these spatially and time-varying vibrating frequencies can potentially be detected on the bridge deck and complicate the precise identification of the hangers with VIVs. Nevertheless, indirect monitoring can readily be applied to existing SHM systems to evaluate the frequency, duration and magnitude of hanger-related VIVs. Owners of large cable-supported bridges can benefit from these ideas because they represent an inexpensive assessment tool to decide whether additional investigations are necessary.

The hangers are not the only bluff bodies that the wind stream encounters. The proposed methodology enables the possibility for investigating other sources of VIVs, such as the direct VIV of the deck. In the particular case of the Hardanger Bridge, the bridge deck was designed and aerodynamically tailored using wind tunnel testing and no VIVs of the deck could be detected.

Conclusion

This document presented the possibility of indirectly detecting and assessing the VIVs of the hangers by analyzing the deck's response. To this end, first, the responses of two hangers were closely inspected, therein achieving excellent correlations between the vortex shedding frequency and the energy content of the acceleration signal. To consider the time-varying nature of wind and the non-stationary nature of the response, adequate TF tools, namely, the CWT and the STFT, were used. Additionally, the direct analysis of the hangers highlighted the strong dependency of the hangers' frequencies on the ambient temperature as well as their particularly low intrinsic structural damping values. Then, the deck accelerations from a permanent SHM system were investigated using the same TF tools. The results showed the same strong and clear correlation between the vortex shedding frequency and signal energy content, confirming that it is possible to indirectly assess hanger VIVs. As expected, the analysis demonstrated that the correlation is stronger in the direction perpendicular to the wind, i.e., the bridge's longitudinal direction. Nevertheless, it was possible to detect not only the Cross-flow VIVs but also the In-line VIVs of the hangers via the indirect analysis of the

deck response. Other phenomena were reported that highlighted the spatial variability of the wind that prompted the presence of multiple vortex shedding frequencies. Finally, this study suggested the possibility to automate the detection of VIVs that consisted of the integration of the STFT results only in the vicinity of the expected vortex shedding frequency.

In summary, the methodology reported here highlights an additional use of existing SHM systems that can readily be implemented. It is possible to assess the frequency and duration of hanger-related VIVs using indirect measurements, such as the deck's accelerations. Because of the complexity of the problem it cannot be used to readily identify problematic hangers, but it constitutes an inexpensive assessment tool to decide whether additional investigations are necessary. The proposed ideas can also be used to detect other sources of VIVs as well as to confirm the performance of any remediation strategy. Furthermore, the analysis in the time-frequency domain provides additional and valuable information on the signals' energy content, thus facilitating the interpretation of the structural response.

Acknowledgements

The research presented in this manuscript was possible thanks to the financial support of The Fjord Crossing research program for the Coastal Highway Route E39.

References

1. Brownjohn JMW, De Stefano A, Xu Y-L, et al.Vibration-based monitoring of civil infrastructure: challenges and successes. *J Civ Struct Health Monit* 2011; 1: 79-95 doi: 10.1007/s13349-011-0009-5.
2. Andersen EJ, Vesterinen A. Structural health monitoring systems. COWI A/S and Futurtec OY, http://www.shms.dk (2006, accessed 7 February 2017).
3. Li H, Ou J. The state of the art in structural health monitoring of cable-stayed bridges. *J Civ Struct Halth Monit* 2016; 6: 43-67 doi: 10.1007/s13349-015-0115-x.
4. Larsen A, Larose GL. Dynamic wind effects on suspension and cable-stayed bridges. *J Sound Vib* 2015; 334: 2-28. doi: 10.1016/j.jsv.2014.06.009.
5. Caetano E. *Cable vibrations in cable-stayed bridges*. Zürich, Switzerland: ETH Hönggerberg, 2007.
6. Kusuhara S , Fumoto K , Yamada I, et al. Wind-induced vibrations and countermeasures for cable systems on long-span bridges. Bridge maintenance, safety management, health monitoring and informatics. In: *IABMAS '08 Proceedings of the Fourth International IABMAS Conference* (eds H-M Koh, D M Frangopol), Seoul, Korea, 13-17 July 2008. Taylor & Francis. doi: 10.1201/9781439828434.ch172.
7. Vickery BJ, Basu RI. Across-wind vibrations of structures of circular cross-section. Part I. Development of a mathematical model for two-dimensional conditions. *J Wind Eng Ind Aerodynamics* 1983; 12: 49-73. doi: 10.1016/0167-6105(83)90080-6.
8. Basu RI, Vickery BJ. Across-wind vibrations of structure of circular cross-section. Part II. Development of a mathematical model for full-scale application. *J Wind Eng Ind Aerodynamics* 1983; 12: 75-97. doi: 10.1016/0167-6105(83)90081-8.
9. Wu T, Kareem A. An overview of vortex-induced vibration (VIV) of bridge decks. *Front Struct Civ Eng* 2012; 6: 335-347. doi: 10.1007/s11709-012-0179-1.
10. Williamson CHK, Govardhan R. Vortex-induced vibrations. *Annu Rev Fluid Mech* 2004; 36: 413-455. doi: 10.1146/annurev.fluid.36.050802.122128.

11. Hansen SO. Vortex-induced vibrations – the Scruton number revisited. *Proc Inst Civ Eng Struct Buildings* 2013; 166: 560–571. doi: 10.1680/stbu.11.00018.
12. Huera-Huarte FJ, Bearman PW. Wake structures and vortex-induced vibrations of a long flexible cylinder—Part 1: Dynamic response. *J Fluids Struct* 2009; 25: 969-990. doi: 10.1016/j.jfluidstructs.2009.03.007.
13. Bourguet R, Karniadakis GE, Triantafyllou MS. Vortex-induced vibrations of a long flexible cylinder in shear flow. *J Fluid Mech* 2011; 677: 342-382. doi: 10.1017/jfm.2011.90.
14. Matsumoto M, Daito Y, Kanamura T, et al. Wind-induced vibration of cables of cable-stayed bridges. *J Wind Eng Ind Aerodynamics* 1998; 74–76: 1015-1027. doi: 10.1016/S0167-6105(98)00093-2.
15. Chen W-L, Zhang QQ, Li H, et al. An experimental investigation on vortex induced vibration of a flexible inclined cable under a shear flow. *J Fluids Struct* 2015; 54: 297-311. doi: 10.1016/j.jfluidstructs.2014.11.007.
16. Li H, Laima S, Ou J, et al. Investigation of vortex-induced vibration of a suspension bridge with two separated steel box girders based on field measurements. *Eng Struct* 2011; 33: 1894-1907. doi: 10.1016/j.engstruct.2011.02.017.
17. Ventosa S, Simon C, Schimmel M, et al. The *S*-Transform from a wavelet point of view. *IEEE Transactions Signal Process* 2008; 56: 2771–2780.
18. Main JA, Jones NP. Evaluation of viscous dampers for stay-cable vibration mitigation. *J Bridge Eng* 2001; 6: 385-397. doi: 10.1061/(ASCE)1084-0702(2001)6:6(385).
19.- Fenerci A, Øiseth O. Measured buffeting response of a long-span suspension bridge with numerical predictions based on design wind spectra. J Struct Eng (Accepted for publication).
20. Usmani AS, Rotter JM, Lamont S, et al. Fundamental principles of structural behaviour under thermal effects. *Fire Saf J* 2001; 36: 721-744. doi: 10.1016/S0379-7112(01)00037-6.
21. Maia NMM, Silva JMM. *Theoretical and experimental modal analysis.* Research Studies Press LTD, 1997.
22. Nagarajaiah S, Basu B. Output only modal identification and structural damage detection using time frequency & wavelet techniques. *Earthq Eng Eng Vib* 2009; 8: 583-605. doi: 10.1007/s11803-009-9120-6.
23. Norberg C. Fluctuating lift on a circular cylinder: review and new measurements. *J Fluids Struct* 2003; 17: 57-96. doi: 10.1016/S0889-9746(02)00099-3.
24. Lienhard JH. Synopsis of lift, drag and vortex frequency data for rigid circular cylinders. Bulletin 300. Washington State University, 1966.
25. Gonzalez I, Karoumi R. Analysis of the annual variations in the dynamic behavior of a ballasted railway bridge using Hilbert transform. *Eng Struct* 2014; 60: 126-132. doi: 10.1016/j.engstruct.2013.12.026.